*Journal of Thermal Analysis and Calorimetry, Vol. 59 (2000) 101–120*

*Dedicated to Prof. Edith A. Turi in recognition of her leadership in education*

# PHASE BEHAVIOR OF POLYMER BLENDS

*Guo Qipeng*[1] *and Liu Zhenhai*[2*]

[1]University of Science and Technology of China, Department of Polymer Science and Engineering, Hefei 230026
[2]Changchun Institute of Applied Chemistry, Chinese Academy of Sciences, Changchun 130022 China

## Abstract

The present report deals with some results on phase behavior, miscibility and phase separation for several polymer blends casting from solutions. These blends are grouped as the amorphous polymer blends, blends containing a crystalline polymer or two crystalline polymers. The blends of PMMA/PVAc were miscible and underwent phase separation at elevated temperature, exhibited LCST behavior. The benzoylated PPO has both UCST and LCST nature. For the systems composed of crystalline polymer poly(ethylene oxide) and amorphous polyurethane, of two crystalline polymers poly(ε-caprolactone) and poly[3,3,-bis-(chloromethyl) oxetane], appear a single $T_g$, indicating these blends are miscible. The interaction parameter $B$'s were determined to be –14 J cm$^{-3}$, –15 J cm$^{-3}$ respectively. Phase separation of phenolphthalein poly(ether ether sulfone)/PEO blends were discussed in terms of thermal properties, such as their melting and crystallization behavior.

**Keywords**: miscibility, phase behavior, phase separation, polymer blend

## Introduction

There has been considerable interest in the study of polymer blends because of their importance in academic and technical aspects. Particularly, much attention has been paid to miscibility and phase behavior in polymer blends [1–3]. Many techniques can be used to study the miscibility and phase behavior of polymer blends. Of them, the calorimetric approach has been demonstrated to be powerful [4–6].

In order to investigate miscibility and phase behavior of polymer blends, differential scanning calorimetry (DSC) has been frequently used for: (1) determination of the glass transition temperature ($T_g$). Generally, the use of $T_g$ in determination of polymer miscibility is based on the judgement that the observation of a single $T_g$ between those of pure components is taken as the evidence of miscibility, although strictly speaking, a single $T_g$ is only indicative of state of dispersion, whereas the appearance of two $T_g$'s suggests the occurrence of phase separation. In miscible amorphous blends, the evolution of two phases when the miscibility

* Author to whom all correspondence should be addressed.

*1418–2874/2000/ $ 5.00*
*© 2000 Akadémiai Kiadó, Budapest*
*Akadémiai Kiadó, Budapest*
*Kluwer Academic Publishers, Dordrecht*

gap is entered as a function of annealing temperature and time allows the calculation of composition of the two phases formed, and thus phase boundary curve can be determined by DSC. (2) Measurement of crystalline melting temperature ($T_m$). Many miscible polymer blends have at least one component that can be crystallized in the blend [1–3]. Blending with a miscible amorphous polymer affects the crystallization of the crystalline polymer. Such blends exhibit both a single compositionally dependent $T_g$ corresponding to mixed amorphous phase and a composition dependent $T_m$ corresponding to a crystalline phase. The interaction energy density $B$, a most important factor determining polymer-polymer miscibility, can be obtained simply and rapidly by thermal measurements of the reduction of crystalline $T_m$. (3) Measurement of other thermal properties. For the blends containing at least one crystalline component, it becomes difficult to follow the appearance of phase separation in an isothermal treatment or in a temperature scan since the magnitude and position of $T_g$ can be strongly affected by the state of crystallization before or after the occurrence of phase separation. However, the changes of other thermal properties, such as the enthalpy of crystallization and fusion, temperature of crystallization and melting, can give some information on phase behavior, which can be taken as an indication of phase separation.

## Experimental

### *Materials*

The blend samples were prepared by casting from solutions of polymer pairs:

PMMA poly(methyl methacrylate), PVAc poly(vinyl acetate), APPO benzoylated *p*-phenylene oxide, PS polystyrene, PBPI-E polyimide of biphthalic anhydride and oxydianiline, PTI-E polyimide of thio-diphthalic anhydride and oxydianiline, PEO polyethylene oxide, PU polyurethane, PCL poly(ε-caprolactone), Penton poly(3,3-bischloromethyl)oxetane, PES-C phenolphthalein poly(etherethersulfone)

### *Methods*

DSC measurements were performed in Perkin Elmer DSC-7 or DSC-2C at heating rate of 20°C $min^{-1}$ under a dry nitrogen atmosphere. DSC curves were recorded by second run to remove effect of thermal history. The temperature and calorimetric scales were calibrated with melting of indium.

The Dynamic Mechanical Analysis (DMA) measurements were carried out by using DuPont 982 model DMA with a heating rate of 5°C $min^{-1}$. The test samples used for DMA were about 2 mm thick, compression molded in the temperature range of 330–380°C. The experimental condition, specification and source of samples, solvent used for casting are detailed in the following section and in quoted references.

## Results and discussion

*Miscibility and phase separation in amorphous polymer blends*

The most commonly used method for establishing miscibility in polymer blends is through the determination of glass transition by DSC. Most miscible polymer blends are amorphous [1–3]. A miscible polymer blend possesses a homogeneous amorphous phase and hence will exhibit a single glass transition temperature ($T_g$) between the $T_g$'s of the components.

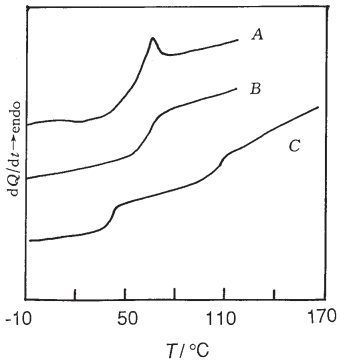


**Fig. 1** DSC curve for 50/50 (mass ratio) PMMA/PVAc blend cast from chloroform. (A) First scan; (B) after heating to 117°C; (C) after heating to 227 °C. The weight-average molecular weight ($M_W$) of PMMA is 60,000. The $M_W$ of PVAc is 453,000

Figure 1 shows DSC curves for a 50/50 poly(methyl methacrylate) (PMMA)/poly(vinyl acetate) (PVAc) blend cast from chloroform [7]. The blend exhibits a single $T_g$ intermediate between those of PMMA and PVAc (see curves *A* and *B*). The heat capacity overshoot in the first scan (curve *A*) is the result of sub-$T_g$ annealing at the drying temperature. The first scan erased the overshoot. However, the DSC curve after heating to 227°C exhibits two $T_g$'s (curve *C* ), which is the result of phase separation. Other compositions show similar DSC curves. All the PMMA/PVAc blends were found to be miscible at low temperature over the entire blend composition range having single composition-dependent $T_g$'s and exhibited phase separation on heating, i.e. lower critical solution temperature (LCST) behavior. The temperature at which the first faint opalescence appeared on heating was designated as the cloud point [7].

All the PMMA/PVAc blends cast from chloroform were transparent at room temperature and were found to undergo phase separation at elevated temperatures. The cloud point curves are shown in Fig. 2. An increase in the molecular weight of PVAc decreases the cloud point temperature as expected. The minimum in the cloud point curve appears close to a 50/50 PMMA/PVAc mass ratio (compositions of blends were expressed by mass ratio or mass fraction in this paper). This composition

varies relatively little with molecular weight, as the molecular weight of PVAc is varied from 20,000 to 453,000.

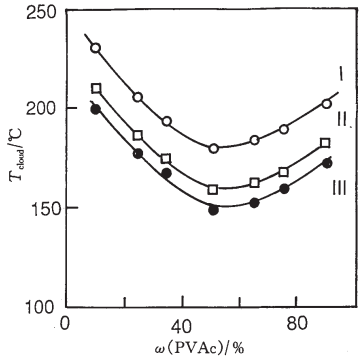


**Fig. 2** Plots of cloud points *vs.* composition for PMMA/PVAc blends. The weight-average molecular weight ($M_W$) of PMMA is 60,000. The $M_W$ of PVAc: (I) 20,000, (II) 170,000 and (III) 453,000

In the presence of a Friedal–Crafts catalyst, the benzoylated PPO (APPO) was prepared by the reaction of PPO with benzoyl chloride and phase behavior for blends of APPO and polystyrene (PS), the molecular weight of PS is $19.0\times10^4$, were observed [8]. When molar fraction of benzoylation degree for APPO is more than 49% APPO-PS blends show two $T_g$ in the DSC curves, and the blend system was found to exhibit both UCST and LCST behavior (Figs 3 and 4).

The miscibility of polyimide (PBPI-E)/polyimide (PTI-E) blends prepared by solution blending was studied by DSC and DMA technigues [9]. The chemical structures of PTI-E and PBPI-E are as follows:

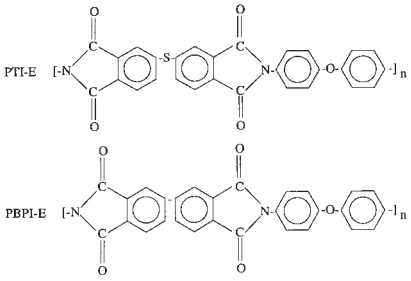


For determination $T_g$ of PBPI-E/PTI-E blends DMA is more sensitive method than DSC (Figs 5a and 5b). It can be clearly seen that two transition peaks in DMA curves, a wider β transition and other α transition ($T_g$), were observed in all composition ranges. The results obtained indicate that the blends are miscible for all compositions.

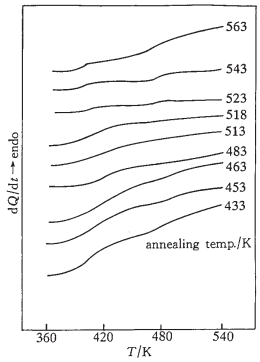


**Fig. 3** DSC curves of APPO-PS (mass ratio 50:50) annealed at different temperatures for 20 min

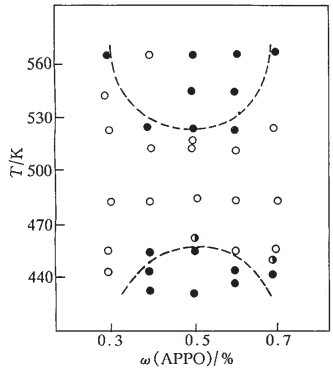


**Fig. 4** Phase diagram of APPO-PS blend system

*Miscible blends containing a crystalline polymer*

Miscibility of blends containing at least one crystalline component shows that they exhibit homogeneity in the amorphous phase, even if one or two separate crystalline phases are formed and even if the each crystalline phase contains only one polymer. Based on this definition, a larger number of blends composed of an amorphous polymer and a semicrystalline polymer have been judged to be miscible [10–12].

The thermal history has a profound influence on DSC curves of polymer blends containing at least one crystalline component. In order to obtain $T_g$ by DSC experiments, the samples are usually first heated up to a temperature between the phase separation temperatures and the melting point of crystalline component and held for several minutes to remove the thermal history.

Figure 6 shows DSC curves (second heating) for miscible blends composed of poly(ethylene oxide) (PEO) and an amorphous polyurethane (PU) [13]. The DSC curves clearly reveal a single glass transition temperature which varied with overall

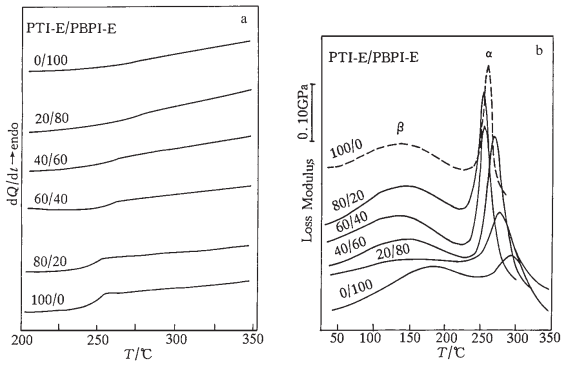


**Fig. 5** DSC (a) and DMA (b) curves of PTI-E/PBPI-E blends

blend composition. The appearance of a single $T_g$ strongly suggests that the blend presents a homogeneous single amorphous phase, i.e. the two components are miscible in the amorphous phase.

The results of $T_g$ of PEO/PU blends as a function of composition are given in Fig. 7, the full curve is as predicted by the Fox equation [14]. The overall $T_g$ variation indicates that these polymers are completely miscible at all compositions. The deviation of experimentally obtained $T_g$'s from the Fox equation at high PEO contents is due to crystallization during quenching. Crystallization for high PEO-content blends was sufficiently rapid for it to be complete during the quenching after the first heating.

By measuring the area under the melting peak of DSC curves, it should be possible to evaluate the heats of fusion ($\Delta H_f$) and crystallization ($\Delta H_C$) in the blend. The fractional crystallinity $X_C$ was calculated from [15]:

$$X_C = (\Delta H_f - \Delta H_C)/\Delta H_f^0 \quad (1)$$

where $\Delta H_f^0$=205 J g$^{-1}$ is the heat of fusion for 100% crystalline PEO [16]. Because of this crystallinity, the mass fraction of PEO in the amorphous phase, ω′, does not equal the overall mass fraction of PEO in the blend, ω. These quantities are related by [15]:

$$\omega' = (\omega - X_C)/(1 - X_C) \quad (2)$$

The open circles in Fig. 7 represent a replot of the $T_g$ values *vs*. the amorphous fraction of PEO. These data conform well to the Fox equation whereas the plot *vs*. overall PEO content does not.

Figure 8 gives the application of the Hoffman–Weeks procedure [17] used to separate the morphological effect on the melting point depression and to determine the equilibrium melting point of PEO in the blend and in the pure state. As shown by the figure, the observed melting temperature ($T_m'$) of PEO and the PEO/PU blends increases linearly with the crystallization temperature for a wide range of undercooling.

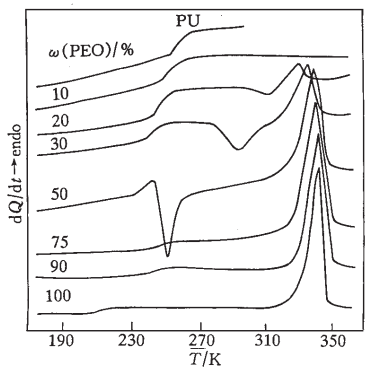


**Fig. 6** DSC curves for PEO/PU blends

A depression of $T_m'$, for the same $T_C$, is observed for blends. The analysis is based on the relationship:

$$T_m' = T_m(1 - 1/\gamma) + T_C/\gamma \quad (3)$$

where $T_m$ is the equilibrium melting temperature, $T_m'$ is the observed melting point of PEO and $T_C$ is the crystallization temperature where annealing of the blends was performed. $1/\gamma$ is a morphological factor [18]. As shown in Fig. 8 the lines $T_m'$–$T_C$ extrapolate to values of $T_m$ that decrease with increased content of PU. The values of the slopes $1/\gamma$ of the lines are almost independent of composition.

The findings that the morphological and stability parameter $1/\gamma$ is almost constant and independent of blend composition and the lines $T_m'$–$T_C$ extrapolate to different equilibrium melting points strongly suggest that the melting point depression can be primarily ascribed to the diluent effect of the non-crystallizable polymer as two components are miscible in the melt.

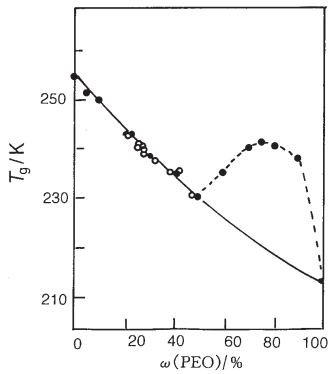


**Fig. 7** $T_g$ for PEO/PU blends plotted *vs*. overall blend composition (•) and *vs*. calculated amorphous phase composition (o). The full curve is as predicted by the Fox equation [14]

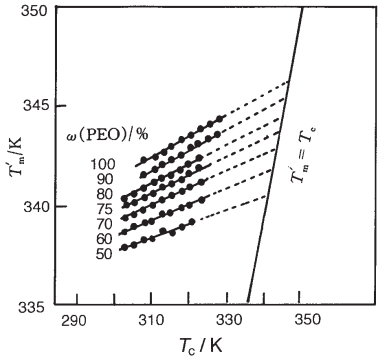


**Fig. 8** Hoffman–Weeks plot to obtain equilibrium melting point for PEO in blends with PU. All samples quenched from 100°C to $T_C$ and crystallized at $T_C$ for 24 h

From this plot and extrapolating $T_m^{'}$ to $T_C$, one obtains the $T_m$ and $T_m^0$ values as plotted in Fig. 9, as suggested by the Nishi–Wang equation [19]:

$$(1-T_m/T_m^0) = -B\,\phi_1^2\,(V_{2U}/\Delta H_{2U}) \quad (4)$$

to obtain the interaction parameter $B$. In this equation, $T_m^0$ is the equilibrium melting temperature of the pure crystalline PEO, $T_m$ is the value for a blend containing $\phi_1$ volume fraction of the amorphous component, and $(\Delta H_{2U}/V_{2U})$ characterizes the heat of fusion per unit volume for 100% crystalline PEO. $(\Delta H_{2U}/V_{2U})$ value was computed from the following literature values [20]: $V_{2U}$=38.9 cm$^3$ mol$^{-1}$ and $\Delta H_{2U}$=8790 J mol$^{-1}$. The slope of the linear relation in Fig. 9 gives a value for $B$ of –14 J cm$^{-3}$.

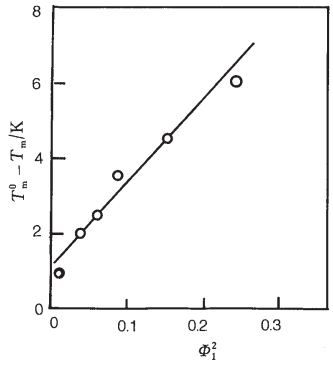


**Fig. 9** Melting point depression analysis to obtain interaction energy density $B$ for PEO/PU blends. Slope gives $B$= –14 J cm$^{-3}$

The negative values found for $B$ in the case of PEO/PU blends support the idea that these polymers are is miscible in the molten state and the fact that the intercept of the Nishi–Wang plot is close to zero indicates that entropic effects contribute little to $B$.

*Miscible blends containing two crystalline polymers*

Both poly(ε-caprolactone) (PCL) and poly[3,3-bis(chloromethyl)oxetane] (Penton) are crystalline polymers and the thermal behaviour of the blends was investigated as a function of composition by using DSC [21].

DSC curves of the quenched samples shown in Fig. 10 reveal a single glass transition temperature which varied with blend composition as indicated by the full circles in Fig. 11. The appearance of a single $T_g$ strongly suggests that the blend presents a homogeneous single amorphous phase, i.e. the two components are miscible in the amorphous phase. Figure 11 exhibits further the $T_g$-blend composition relationship evaluated according to the Fox equation [14]. The experimental data conform well to the Fox equation. This further indicates that these two polymers are completely miscible at all compositions. Figure 10 also shows the melting endotherms for both PCL and Penton, and crystallization exotherms for both PCL and Penton were observed for some blends with due compositions.

Figure 11 also shows the $T_C$ and $T_m$'s of both polymers of the quenched samples as fuctions of blend composition. For the pure PCL, no crystallization exotherm was observed as seen in Fig. 10 since crystallization was sufficiently rapid to occur completely during the quenching. However, for the blends with Penton content up to 60%, crystallization exotherm occurs and $T_C$ increases with increase of Penton content. This phenomenon implies that the crystallization of PCL in the blend becomes progressively difficult with increasing Penton content. Furthermore, the blend containing 80% Penton did not show any crystallization exotherm of PCL. It is also noted that crystallization of Penton did not occur in the blends with Penton content lower than 40%. The decrease in crystallization rates of both PCL and Penton in blends was also observed in the crystallization process during the cooling run. Figure 12 summarizes the $T_C$ data obtained as a function of blend composition. It can be seen that the $T_C$ of PCL decreases with Penton content, which means that the crystallization rate of PCL decreases with Penton content. At same time, the $T_C$ of Penton decreases with

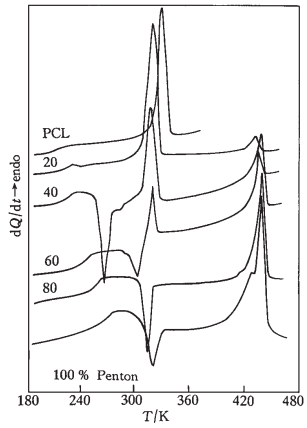


**Fig. 10** DSC curves for the quenched samples of PCL/Penton blends

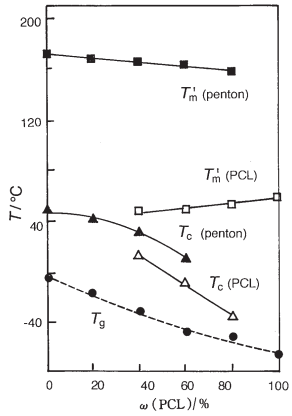


**Fig. 11** Thermal transition behavior of PCL/Penton blends. All the samples were first melted at 200°C and then rapidly quenched to –133°C. The broken curve is calculated according to the Fox equation [14]

increasing PCL content, suggesting that the crystallization rate of Penton in the blend decreases with PCL content. This result is as expected for miscible blends containing crystalline components.

The crystallinity index of PCL phase, $X_C$(PCL), and the Penton phase, $X_C$ (Penton), in the PCL/Penton blends are presented in Fig. 13 as functions of blend composition. The filled symbols in the figure denote the quenched samples, and the open symbols the as-cast samples. The following facts can be seen from the figure. First, the values of both the $X_C$(PCL) and the $X_C$ (Penton) for the as-cast samples are all higher than those for the quenched samples. Second, the $X_C$(PCL) for both the quenched and the as-cast samples begins to rapidly decrease with Penton content at 60/40 PCL/Penton composition. This could be considered to be due to the enhanced $T_g$ value of the blend. Finally, we note that the $X_C$ (Penton) values do not decrease

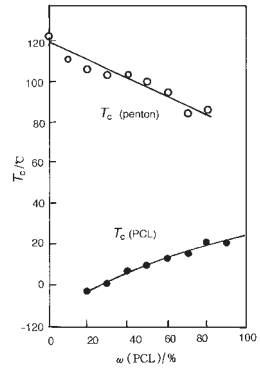


**Fig. 12** Non-isothermal DSC crystallization temperature ($T_C$) of Penton (open circle) and PCL (closed circle) as a function of blend composition

with the addition of PCL. This is because the $T_g$ of the system does not increase with increasing PCL content.

The interaction energy density $B$ for the PCL/Penton blends was estimated to be –15 J cm$^{-3}$ by using the Nishi–Wang plot [19] from the equilibrium melting point depression data. The negative $B$ value confirms that these polymers are miscible in the molten state.

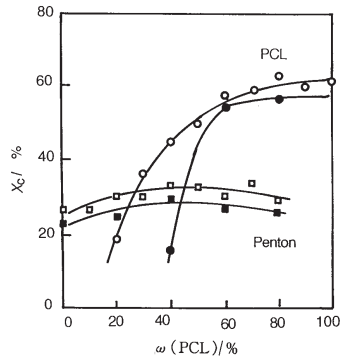


**Fig. 13** Crystallinity index $X_C$ of PCL (circle) and Penton (squares) as a function of blend composition. The filled symbols denote the quenched samples, and the open symbols the as-cast samples

*Phase separation in crystalline polymer blends*

For the blends containing one (or more) crystallizable component, it becomes difficult to follow the appearance of phase separation in an isothermal treatment or in a temperature scan since the magnitude and position of $T_g$ can be strongly affected by the state of crystallization before or after the occurrence of phase separation. However, the changes of other thermal properties, such as enthalpy of crystallization and fusion, temperature of crystallization and melting, can give some information on phase behavior, which can be taken as an indication of phase separation. Here, we exhibit an investigation of the phase behaviors in crystalline/miscible blends consisting of PEO and phenolphthalein poly(ether ether sulfone) (PES-C) [22]. In this system, it was difficult to determine the phase boundary, i.e. a temperature *vs.* composition phase diagram by using DSC to follow appearance of two separate $T_g$'s at a certain annealing temperature as conventionally shown in amorphous polymer blend systems, since PEO is a crystalline polymer with a typically high degree of crystallinity. However, the change of other thermal properties as functions of annealing temperatures can give some significant information, and the phase diagram was determined based on the analysis of thermal properties.

The miscible PES-C/PEO blends were prepared by solution casting from *N*,*N*-dimethylformamide, and they were used throughout this study. The PES-C/PEO blends with ω(PEO)<50% were transparent at room temperature, but the blend samples containing ω(PEO)=50% and more increasingly became opaque with increase of

PEO content. The polarizing microscopic observation of all these blends with ω(PEO)>50% shows the typical morphology of spherulites. Heated up to 80°C, i.e. above the melting point of PEO(65°C), these opaque films all became clear. This observation indicates that the PES-C/PEO blends present a single homogeneous amorphous phase, i.e. phase separation did not occur, at least on a scale with dimension of phase domains exceeding the wavelength of visible light.

When further heated up to 200°C, all the initially clear samples became turbid in succession, but the remixing did not occur when these samples were cooled due to kinetic effects. Careful microscopic observations revealed that the turbidity was caused by the formation of a phase-separated structure. These results suggest that the PES-C/PEO blends display a LCST behavior, which means that there is a negative enthalpic contribution of mixing.

Figure 14 shows DSC curves of PES-C/PEO blends. It can be seen that each blend displays a single glass transition temperature ($T_g$), intermediate between those of the two pure components and changing with the blend composition. According to the transparency of the sample and glass transition behavior, the conclusion can be reached that the PES-C/PEO blends are completely miscible in the amorphous state, i.e., possess a single, homogeneous, amorphous phase for all compositions below the temperature of phase separation. Figure 15 shows the plots of the thermal transitions of the blend as functions of mass fraction of PEO. For the plot of $T_g$'s *vs*. PEO mass fraction, the composition of the amorphous phase was calculated after subtracting the crystallinity of PEO. The prediction $T_g$ of Gordon–Taylor equation [23], using a $k$ value of 0.24, is also presented in Fig. 15, fitting the experimental data quite well.

As can be seen in Fig. 14, no cold crystallization exotherm was observed for the pure PEO and the 20/80 PES-C/PEO blend, since crystallization was sufficiently rapid to occur completely during the quenching. However, for the blends with PES-C content from 30% to 50%, the crystallization temperature ($T_C$) increases with increasing PES-C content. This phenomenon indicates that crystallization of PEO becomes progressively difficult in the PES-C rich blends. Furthermore, the blends with PES-C

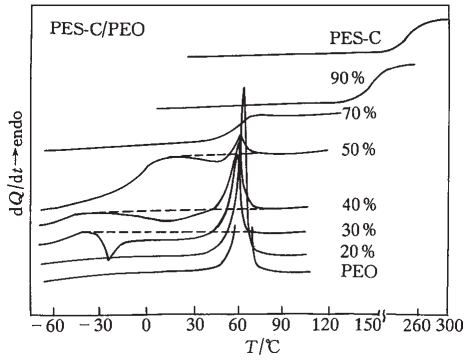


**Fig. 14** DSC curves of PES-C/PEO blends with different blend composition after quenching. Heating rate 20°C $min^{-1}$. For easy comparison all curves are normalized to 1 mg of sample

content of 70% or higher did not show any crystallinity. It was noted that the $T_m$ of PEO in the blends apparently decreases with addition of PES-C to the system, which indicates that PES-C hinders the crystallization of PEO in the blends. This is typical characteristic of a miscible blend composed of an amorphous polymer and a crystallizable polymer in which the $T_g$ of the amorphous polymer is higher than that of the crystallizable component.

The interaction energy density $B$ for the PES-C/PEO blends was estimated by using the Nishi–Wang plot [19] from the apparent melting point depression data. A tentative value of $B$ was found to be –17 J cm$^{-3}$ at 65°C for the PES-C/PEO. The negative $B$ value suggests the negative free energy of mixing. It has to be stressed that this estimate may be subject to some errors since the morphological effect on the melting point depression has not been excluded.

Figure 16 shows the crystallinity of PEO as a function of blend composition. The crystallinity of PEO in the blends containing PES-C less than 20% does not deviate much from the dashed line (Fig. 16), which stands for the crystallinity of PEO in the blends if the crystallization process is not influenced by the presence of PES-C. However, there is a dramatic decrease in crystallinity when the content of PES-C is more than 20%, indicating a pronounced inhibition of crystallization by the presence of PES-C.

All these results clearly show that PES-C/PEO blends are miscible and exhibit an LCST behavior. However, as shown above, there are different thermal behaviors for the miscible blends of PES-C and PEO, depending on the blend composition. Blends with different composition display different changes of thermal properties while phase separation occurs. Therefore, the investigation of phase separation should be performed in the light of the blend compositions. The studies of the phase separation process are discussed in detail as follows.

All the PES-C/PEO blends containing less than 50% PEO do not show crystallization phenomena under the experimental conditions (Fig. 14). Herein, the results of DSC measurement for the 70/30 PES-C/PEO blends were representatively described based on the evolution of thermal properties as a function of annealing temperature. A series of DSC curves of the 70/30 PES-C/PEO blends was obtained after annealing

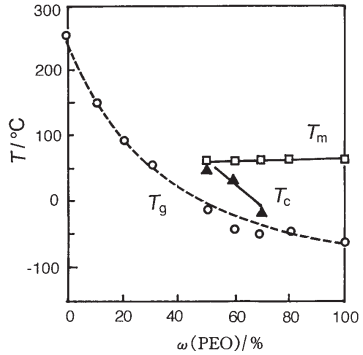


**Fig. 15** Transition behavior of PES-C/PEO blends. The dashed line was drawn from the Gordon–Taylor equation with $k$=0.24

at temperature between 80 and 200°C and then quenching to –70°C (Fig. 17). It can be seen that when annealed below 110°C, the DSC scans show no obvious changes, but a significant difference was observed as the annealing temperature is higher than 110°C. Minor melting peaks of PEO in the DSC heating curves appear, and the area under the melting peaks increases with increasing annealing temperature, reaching a plateau when the annealing temperature is higher than 140°C (Fig. 18). The melting

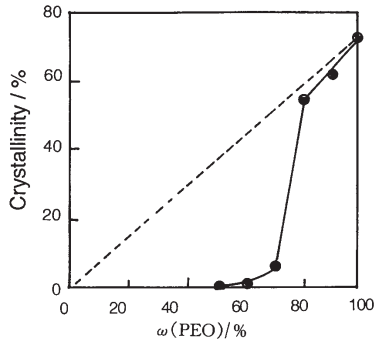


**Fig. 16** Percent crystallinity of PEO in PES-C/PEO blends from the scans after annealing at 80°C for 5 min and then quenching. The dashed line represents the crystallinity of PEO in blends if the crystallization process was not influened by the presence of PES-C

temperature ($T_m$) increases dramatically after annealing up to 110°C and thereafter only gradually increases (Fig. 18). The appearance of the crystallization of PEO in the blends is indicative of the occurrence of phase separation, i.e., the PEO-rich phase has separated from the initial homogeneous amorphous PES-C/PEO mixture. With phase separation taking place, PEO gradually concentrates from the original homogeneous blends and both the PEO-rich phase and PEO-lean phase are simultaneously formed, resulting in the appearance of the crystallization and fusion of PEO during the process of quenching and heating. The higher the annealing temperature, the larger the area under the melting peaks, which suggests that the phase separation occurs more completely. Hence, the occurrence of the melting at a particular annealing temperature should be considered as the beginning of phase separation.

From Fig. 17, it is observed that $T_g$'s of the blends became broad in the vicinity of the onset of phase separation. The width of the glass transition may reflect the magnitude of local compositional fluctuations in the polymer blends, implying the relative homogeneity or miscibility of the system. However, the transition temperature do not change until the appearance of minor melting peak in the DSC curve, indicating the occurrence of phase separation. With the phase separation occurring, the $T_g$'s gradually shift to lower temperatures, although they increasingly became indistinguishable at higher annealing temperatures due to its higher crystallinity after more complete phase separation. It is noted that the second $T_g$, i.e. that of the PES-C rich phase, cannot be seen in Fig. 17. However, there is an apparent deviation of DSC curves from the baseline after the melting peaks of PEO. The higher the annealing temperature, the larger the deviation, which

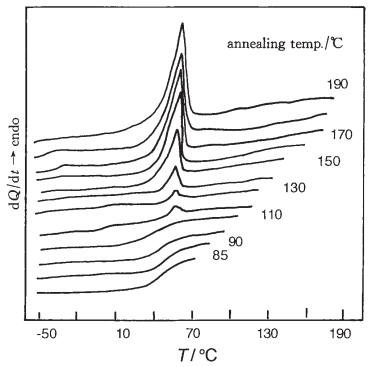


**Fig. 17** DSC curves of the 70/30 PES-C/PEO blend for various annealing temperatures between 85 and 195°C. The annealing time was 5 min

suggests a broaden range of glass transition of the PES-C-rich phase after the multistage thermal treatment. It should be pointed out that the heating rescans after the appearance of the melting peaks of PEO do not show the cold crystallization of PEO, which indicates that the crystallization of PEO in the newly separated PEO-rich phase mainly occurs during quenching process.

For the PES-C/PEO 50/50 blends, the amorphous and homogeneous mixture was obtained after quenching from 80°C to –70°C in terms of the comparison of the area under the crystallization and melting peaks, since there are equal values of the enthalpy between the two transitions. Figure 19 shows a series of heating DSC curves of the 50/50 PES-C/PEO blend annealed at different temperatures between 80 and 130°C. Below 105°C, the endothermic enthalpy remains unchanged and equal to exothermic enthalpy, which indicates that PEO crystallizes only during the heating run of DSC after quenching. When the annealing temperature is 105°C or above, both the enthalpy values began to increase dramatically, and the enthalpy of fusion even began to surpass that of crystallization in contrast to the cases at the annealing temperatures below 105°C. At the same time, the cold crystallization temperatures ($T_c$) shifted to lower temperatures whereas the melting temperatures ($T_m$) increased.

These results clearly show that, at annealing temperatures above 105°C, PEO began to crystallize not only during the heating scan but also during the quenching process. The shift of the crystallization peaks to lower temperatures indicates that the composition might have changed somewhat during annealing. In other words, on annealing, two separated amorphous phases are formed, i.e., one is the PES-C rich phase whereas the other corresponds to the PEO-rich phase. The PEO-rich phase can crystallize during the quenching process, and its thermal behavior is similar to that of the 30/70 PES-C/PEO blend (Fig. 14). The cold crystallization of PEO occurs more easily, i.e. the hindrance effect of PES-C on PEO crystallization becomes smaller because the content of the amorphous component (PES-C) with higher $T_g$ in the newly formed PEO-rich phase reduces. As a consequence, the enthalpy values of crystallization and fusion increased, and $T_m$ increased since more perfect crystals could be

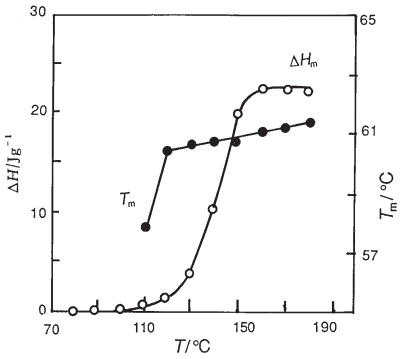


**Fig. 18** Variation of thermal properties with annealing temperature for the 70/30 PES-C/PEO blend

formed. It is assumed that the shift of the crystallization peak at a particular annealing temperature can correspond to the beginning of phase separation. Of course, the annealing time is an important factor which affects the shift and magnitude of the crystallization peak after the phase separation occurs. The one-phase temperature zone is reserved only if every parameter remain constant: $\Delta H_f$, $\Delta H_c$, $T_c$ and $T_m$ (Fig. 20).

When the PEO content in the blends was more than 50%, only the crystalline blends were obtained under the experimental condition used since PEO crystallization can occur during the quenching process, and at the same time there was cold crystallization phenomenon during the heating scan. With increasing of PEO content, the cold crystallization peak in the heating DSC curves became fairly indistinguishable when PEO was more than 80% in the blends. Representatively, Fig. 21 gives a series of DSC curves of the 30/70 PES-C/PEO blend annealed at different temperatures ranging from 85 to 110°C. It is observed that the thermal enthalpy values of crystallization and melting transition change depending upon the annealing temperature.

The plot of thermal enthalpy of crystallization and fusion as a function of annealing temperature is shown in Fig. 22. It is noted that, at or below 80°C, the two enthalpy values almost remain constant, which indicates that the composition of the blends does not change during the annealing process, and the phase separation does not take place. However, when the annealing temperature is above 80°C, the enthalpy of crystallization gradually decreases with increasing annealing temperature, whereas the enthalpy of fusion increases. It is reasonable to believe that the changes of thermal enthalpy are caused by the occurrence of phase separation during annealing. Therefore, the phenomenon is indicative of the occurrence of phase separation. With increasing annealing temperature, the area under the melting peaks became larger whereas the enthalpy of crystallization became smaller and smaller. When the annealing temperature is 110°C or higher, the thermal behavior is similar to that of pure PEO, suggesting that complete phase separation has occurred. In addition, it was observed that, in this case, the $T_m$ is relatively independent of the annealing temperature, as shown in Fig. 22.

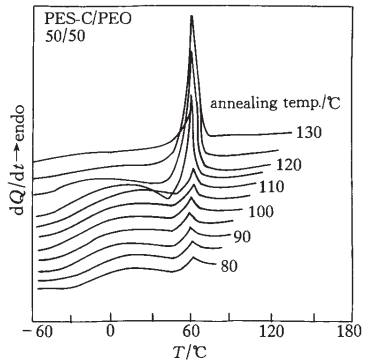


**Fig. 19** DSC curves of the 50/50 PES-C/PEO blend for various annealing temperatures between 80 and 130°C. The annealing time was 5 min

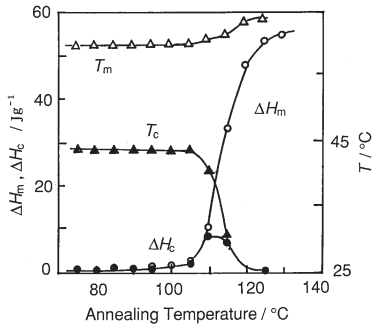


**Fig. 20** Variation of thermal properties with annealing temperature for the 50/50 PES-C/PEO blend

On the basis of this analysis of thermal properties, the temperature of phase separation were determined and a phase boundary diagram was established, as shown in Fig. 23. The optical microscopic observation was also applied to obtain the cloud point curve. It can be seen from the figure that the temperatures determined by optical observation were slightly higher than those determined by thermal analysis. However, the phase diagram determined with the two approaches agree well. The asymmetrical phase diagram has a minimum around 20% PES-C and the system exhibits typical LSCT behavior. We have demonstrated here that the changes of thermal properties of blends composed of a crystalline polymer and an amorphous polymer can provide information about the occurrence of phase separation, and thermal analysis can be used to determine the phase boundary of such blends.

DSC analysis provides a rapid means of assessing the miscibility and phase behavior of small samples of polymer blends, and it has found increasing application in the study of polymer blends. Recently, the measurements of heat of demixing by DSC have been carried out in several miscible polymer blend systems [24–28]. For

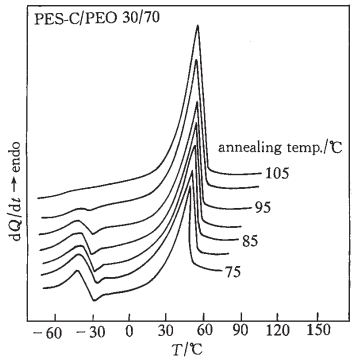


**Fig. 21** DSC curves of the 30/70 PES-C/PEO blend for various annealing temperatures between 85 and 110°C. The annealing time was 5 min

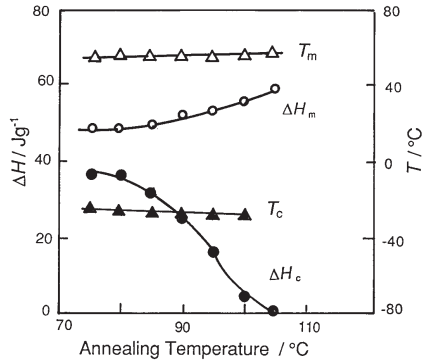


**Fig. 22** Variation of thermal properties with annealing temperature for the 30/70 PES-C/PEO blend

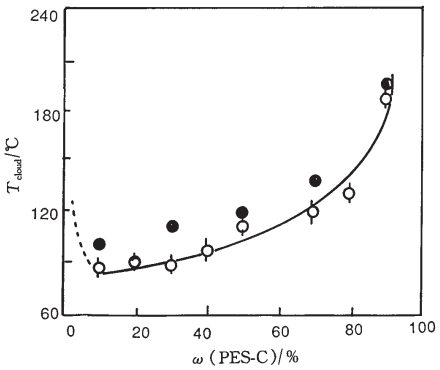


**Fig. 23** Phase diagram of PES-C/PEO blends. Cloud points were determined by microscopic observation (closed circle), and demixing temperature by DSC (open circle)

the polymer blends with high molecular weight, the combinatorial entropy of mixing ($\Delta S_{mix}$) is negligible and the free volume contribution further increases the free energy of mixing ($\Delta G_{mix}$). As a result, the miscibility depends on the heat of mixing ($\Delta H_{mix}$). Therefore, the measurement of heat of mixing can play an important role in predicting miscibility in polymer blends. However, the direct measurement of heat of mixing is less successful, and at the same time, some indirect methods to estimate $\Delta H_{mix}$ or miscibility [29–31] may not always give reliable results. DSC studies by several authors [24–28] have revealed that some miscible polymer blend systems show an endothermic (or exothermic) effect resulting from demixing of components. The concentration and temperature dependences of the heat of demixing and the excess heat capacity of the polymer blends were obtained by using DSC analysis, so that spinodial and bimodal curves were determined. The results have been interpreted and compared with the theoretical predictions of the modern equation-of-state theory [32] and the ten Brinke and Karasz mode [33].

## References


1 D. R. Paul and S. Newman ed. 'Polymer Blends', Academic Press, New York 1978, Vols. 1 and 2.
2 O. Olabishi, L. M. Robeson and M. T. Shaw, 'Polymer-Polymer Miscibility', Academic Press, New York 1979.
3 L. A. Utracki, 'Polymer Alloys and Blends', Oxford University Press, New York 1989.
4 J. F. Fried, in 'Developments in Polymer Characterization-4', (J. V. Dawkins ed.), Applied Scientific Publishers, London 1983. Chapter 2.
5 S. W. Shalaby and H. E. Bair, in 'Thermal Characterization of Polymetric Materials', (E. A. Turi ed.) Academic Press, New York 1981. Chapter 4.
6 Liu Zhenhai and T. Hatakeyama eds. 'Handbook of Analytical Chemistry', Vol. 6, Chemical Industry Press, Beijing 1994, p. 81; T. Hatakeyama and Zhenhai Liu eds. 'Handbook of Thermal Analysis', John Wiley & Sons, Chichester 1998, p. 92.
7 Q. Guo, Polym. Commun., 31 (1990) 217.
8 Yang Xianghong, Huang Yuhui, Zhao Shuliu and Cong Guangmin, Acta Polym. Sinica, 2 (1992) 215.
9 Zhang Ping, Sun Zhenhua, Zhuang Yugang, Ding Mengxian and Feng Zhiliu, Acta Polym. Sinica, 6 (1993) 719.
10 Q. Guo, Macromol. Rapid Commun., 16 (1995) 785.
11 Z. Zhong and Q. Guo, Polymer, 279 (1997) 38.
12 Q. Guo, S. Zheng, J. Li and Y. Mi, J. Polym. Sci. Polym. Chem. Ed., 35 (1997) 211.
13 Q. Guo, H. Xu, D. Ma and S. Wang, Eur. Polym. J., 26 (1990) 67.
14 T. G. Fox, Bull. Am. Phys. Soc., 1 (1956) 123
15 A. C. Fernandes, J. W. Barlow and D. R. Paul., J. Appl. Polym. Sci., 29 (1984) 1971.
16 G. Vidotto, D. L. Levy and A. J. Kovacs, Kolloid Z Z Polym., 230 (1969) 289.
17 J. D. Hoffman and J. J. Weeks, J. Res. Natn. Bur. Stand., 66A (1962) 13.
18 J. D. Hoffman, SPE Trans., 4 (1964) 315.
19 T. Nishi and E. T. Wang, Macromolecules, 8 (1975) 909.

20 D. W. Krevelen, in Properties of Polymers, 2nd Ed., Elsevier Scientific, Amsterdam 1976.
21 Q. Guo, Makromol. Chem., 191 (1990) 2639.
22 S. J. Zheng, Li Y. Huang and Q. Guo, J. Polym. Sci., Polym. Phys. Ed., 35 (1997) 1383.
23 M. Gordon and J. S. Taylor, J. Appl. Chem., 2 (1952) 495.
24 A. Natansohn, J. Polym. Sci. Polym. Lett. Ed., 23 (1985) 305.
25 M. R. W. Ebert, R. W. Gaebella and J. H. Wendorff, Makromol. Chem. Rapid Commun., 7 (1986) 65.
26 S. Shen and J. M. Torkelson, Macromolecules, 25 (1992) 721.
27 J. A. Moore and J. H. Kim, Macromolecules, 25 (1992) 1427.
28 L. C. Cesteros, J. R. Isasi and I. Katime, Macromolecules, 27 (1994) 7887.
29 A. A. Tager, T. T. Scholokhovich and Y. S. Bessanov, Eur. Polym. J., 11 (1975) 321.
30 C. A. Cruz, J. W. Barlow and D. R. Paul, Macromolecules, 12 (1979) 726.
31 C. Zhikuan, S. Ruona, D. J. Walsh and J. S. Higgins, Polymer, 24 (1983) 263.
32 H. Hamada, T. Shiomi, K. Fujisawa and A. Nakajima, Macromolecules, 13 (1980) 729.
33 G. ten Brinke and F. E. Karasz, Macromolecules, 17 (1984) 815.